# Laser-Beam Optimization for Momentum Transfer by Laser-Supported Detonation Waves

N. Ferriter
*Strategic Systems Project Office, Dept. of the Navy, Washington, D.C.*
and
D. E. Maiden,† A. M. Winslow,‡ and J. A. Fleck Jr.§
*University of California, Lawrence Livermore Laboratory, Livermore, Calif.*

**Momentum transfer from a laser-supported detonation wave to a solid target has been studied by means of a time-dependent, two-dimensional, two-temperature Lagrangian hydrodynamics code. Its dependence on laser pulse length has been calculated and pulse length conditions obtained for optimizing impulse transfer to a target of finite area embedded in a larger plane surface, taking into account the laser coupling efficiency. Computer solutions are compared with existing analytical models for laser-induced surface pressures and impulse, and a summary is given of the pulse time regime of applicability of blast-wave models proposed by previous investigators. Scaling laws are given for optimized pulses that predict the laser parameters required to deliver a given impulse to a target of given area in an atmosphere of given density.**

## I. Introduction

WHEN a pulsed high-power laser initiates a laser-supported detonation (LSD) wave at a target surface in an atmosphere, an impulse is delivered to the surface by the hot gas. At sufficiently high laser intensity, this impulse, which is independent of the nature of the surface (except for an initial transient), may become a potent damage mechanism. In order to utilize this impulse, it is necessary to understand how it is related to beam parameters, such as intensity, pulse length, and spot size. An important practical design consideration is the coupling coefficient, defined as impulse delivered to the target per unit of energy in the laser pulse.

Previously published theoretical studies of impulse transfer by LSD waves have been made by several investigators, among them Pirri,[1] who used one-dimensional gasdynamic analysis and a cylindrical blast-wave scaling model, and Nielsen,[2] who employed a two-dimensional Eulerian hydrodynamics code (see Ref. 2 for additional references). Nielsen found agreement between his computed results and Pirri's blast-wave model for the rate of plasma spreading and for the impulse transfer. However, his calculations treated long pulse lengths and effectively infinite targets. We wish to consider instead the following problem: given an infinite plane surface containing a circular target of radius $a$, and a pulsed laser beam of radius $R$ concentric with the target, what values of $R$ and laser pulse length $\tau_p$ will optimize (in some sense to be defined) the impulse transfer to the target area? For this case, which we call "spot loading," we will show that short pulse lengths (about one-third of the radical hydrodynamic relaxation time) are desirable, for which a spherical rather than cylindrical blast-wave model is (in part) appropriate. We have also studied the case considered by Nielsen,[2] which we call "total loading," and find that optimization in this case leads to pulses a factor of three longer, for which cylindrical blast-wave scaling may be used.

Since the pressure relaxation time is much less than the response time of the target, it is possible to treat the expansion of the plasma and the deflection of the target as independent problems. We have used the LASNEX computer model of LSD waves described in an earlier report[3] to study the initiation and propagation of the LSD waves and the impulse delivered to the surface. After LSD waves are initiated, their properties are independent of the target material and the laser wavelength, since the laser energy is all deposited at the LSD wavefront independent of wavelength. Thus one can discuss the resulting pressure loading and momentum transfer with complete generality. Only the response of the target to the induced momentum need then be specified.

We have treated the target response by assuming that a given target can be characterized by the impulse required to make it fail, leaving the failure mode unspecified (for a thin ductile plate this is plastic deformation[4]; for a thick brittle one, cracking[5]). By imposing the optimization conditions developed from our computer calculations, we are able to predict the laser parameters – beam radius, pulse length, and pulse energy – required to deliver a given impulse, and we give typical parameters required for rupture of thin aluminum and steel plates by optimized pulses.

## II. LASNEX Calculations of Surface Pressure and Sound Speed

The LASNEX code[3] is a two-dimensional Lagrangian code, based on a two-temperature nonequilibrium model. The code utilizes detailed thermodynamic data for air and an aluminum target, and a detailed model of the absorption of laser radiation. Calculations have shown excellent quantitative agreement with pulsed laser experiments,[6] giving confidence in the capability of the code for modeling LSD wave phenomena. Among the general relations confirmed by LASNEX code runs is the Raizer formula[7] for the detonation wave speed $D$:

$$D = [2(\gamma^2 - 1) I_0/\rho_0]^{1/3} \tag{1}$$

where $I_0$ is the incident laser intensity, $\rho_0$ is the density of the ambient air, and $\gamma$ is the specific-heat ratio for an assumed perfect gas. LASNEX shows that Eq. (1) is valid for 10.6-$\mu$m radiation and normal-density air over an intensity range extending from about $3\times10^6$ to $2\times10^9$ W/cm$^2$ if the value of $\gamma$ is taken to be 1.18, even though LASNEX is based on a nonequilibrium two-temperature model and utilizes an

Received Sept. 14, 1976; revision received June 24, 1977.
Index categories: Lasers; Shock Waves and Detonations.
*Commander.
†Research Scientist, Mechanical Engineering Department.
‡Physicist, Theoretical Physics Division.
§Associate Division Leader, Theoretical Physics Division.

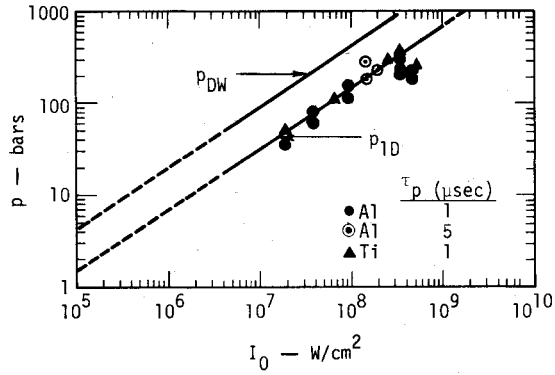


**Fig. 1 Detonation pressure and one-dimensional surface pressure for LSD waves in normal density air vs beam intensity [Eqs. (2) and (3)].**

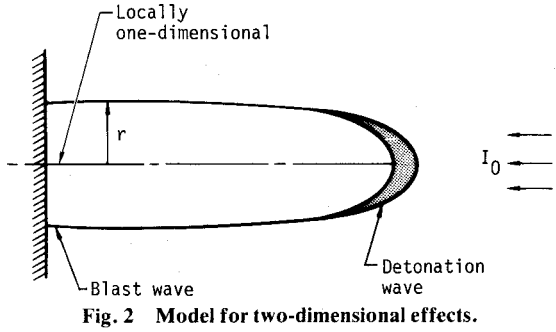


**Fig. 2 Model for two-dimensional effects.**

equation of state having a nonconstant value of $\gamma$. The value $\gamma \approx 1.2$ is in agreement with experimental data for heated air.[1]

A formula has been derived by Grib,[8] Pirri,[1] and Holmes[9] for the pressure on a target surface resulting from a one-dimensional LSD wave traveling away from the target surface. This formula is

$$p_{1D} = [(\gamma+1)/2\gamma]^{2\gamma/(\gamma-1)} p_{DW} \tag{2a}$$

$$p_{DW} = \rho_0 D^2/(\gamma-1) \tag{2b}$$

where $p_{DW}$ is the pressure in the detonation wave. If the value $\gamma = 1.18$, needed for Eq. (1) to apply, is substituted into Eq. (2), the following result is obtained:

$$p_{1D}(\text{bars}) = (6.9\times10^{-4})\,[I_0(\text{W/cm}^2)]^{2/3} \tag{3}$$

Figure 1 shows good agreement of $p_{1D}$ with the experimental data of Hettche et al.[10] On the other hand, the detailed LASNEX calculations yield the following steady-state pressure, after an initial transient peak

$$p_{1D} = (6.35\times10^{-4})\, I_0^{2/3} \tag{4}$$

The LASNEX results also show that over most of the intensity range quoted above the sound speed $c_J$ behind the detonation front is related to the detonation speed $D$ by

$$c_J = \gamma/(\gamma+1)D \tag{5}$$

in agreement with Raizer.[7]

## III. Impulse Delivered and Pulse Optimization

As an LSD wave recedes from the target, the pressure $p(r,t)$ given in Eq. (3) will persist at a radial position $r$ until a sound signal can travel from the edge of the beam to the position $r$ (Fig. 2). At the center of the beam of radius $R$ that pressure will persist for a time

$$\tau_R = R/c_J \tag{6}$$

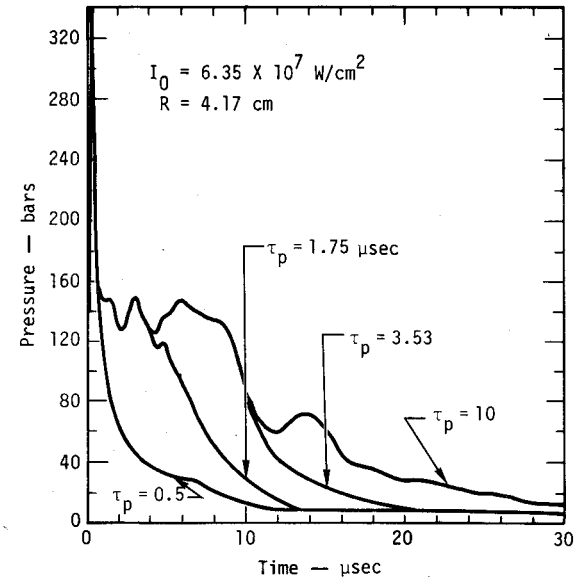


**Fig. 3 Surface pressure history at beam center for various pulse lengths (LASNEX).**

which may be called the radial relaxation time. Although the sound speed varies by a factor of $\gamma$ from the target to the detonation front,[8] use of $c_J$ in Eq. (6) can be shown to be a good approximation.[4]

When the laser beam is turned off at time $\tau_p$, the pressure on the target can also relax as the result of a sound signal traveling from the position of the detonation wave front to the target. After a time $\tau_p$, the LSD wave will have moved a distance $D\tau_p$ away from the surface. A sonic relaxation, commencing at this time, will take approximately a time $D\tau_p/c_J$ to reach the surface. The axial relaxation time, measured from switch-on of the beam, is thus

$$\tau_z = \tau_p + \frac{\tau_p D}{c_J} = \left(\frac{2\gamma+1}{\gamma}\right)\tau_p \tag{7}$$

using Eq. (5), which is the time for the pressure on the target surface to relax one-dimensionally following beam switch-off. The hydrodynamic relaxation time $\tau_H$ will be the smaller of these two times:

$$\tau_H = \min(\tau_R, \tau_z) \tag{8}$$

The relaxation behavior of $p(0,t)$ predicted by the foregoing analysis was verified by LASNEX calculations using a 10.6-$\mu$m beam with $I_0 = 6.35\times10^7$ W/cm², $R = 4.17$ cm, in air with density $\rho_0 = 0.00125$ g/cm³ and $\gamma = 1.18$. The predicted quantities are $c_J = 0.398$ cm/$\mu$sec, $D = 0.736$ cm/$\mu$sec, $\tau_R = 10.5$ $\mu$sec, $p_{1D} = 110$ bars, and $p_{DW} = 311$ bars.

The pressure history at the center of the beam for four values of $\tau_p$ is shown in Fig. 3. An initial pressure peak $p = 340$ bars is seen at $t \approx 0.2$ $\mu$sec, representing the detonation wave directly on the target's surface. As the LSD wave propagates away from the surface, the pressure drops to 135 bars at $t = 1$ $\mu$sec, in reasonable agreement with the calculated one-dimensional value of $p_{1D}$. The difference in the reported result and that obtained from Eq. (4) is due to initial conditions. A 0.1-cm zone of hot air at 1.5 eV was used for the present calculation. The calculated hydrodynamic relaxation time $\tau_H = \min(\tau_R, \tau_z)$ for $p_{1D}$ to begin to decay is shown in Table 1 along with the observed values. The observed times are about 20% less than the calculated values because the pressure is higher than the theoretical value and thus the speed of sound is correspondingly greater. However, the presence of two relaxation times $\tau_z$ and $\tau_R$ is clearly seen. For pulses with $\tau_z > \tau_R$ we see that pressure decay sets in at $\tau_R$ as predicted

**Table 1 Observed and calculated hydrodynamic relaxation time $\tau_H$ for different pulse lengths**

| $\tau_p$ (μsec) | Calculated $\tau_H$ (μsec) | Observed $\tau_H$ (μsec) |
|---|---|---|
| 0.5 | 1.42 (axial) | 1.0 |
| 1.75 | 4.99 (axial) | 4.0 |
| 3.53 | 10.5 (radial) | 8.7 |
| 10.0 | 10.5 (radial) | 8.7 |

although the extra energy provided by longer pulses slows down the rate of pressure decay.

The impulse intensity on the surface due to the pressure $p(r,t)$ is given by

$$I_I(r,t) = \int_0^t p(r,t')\,dt' \tag{9}$$

where $r$ is the radial distance from the center of the beam. The impulse delivered to a target out to a specified radius $r$ may be written, following Pirri, as

$$I_r(t) = p_{ID} A_s \tau_H + 2\pi \int_{\tau_H}^{t_0} \int_0^{r(t)} p(r,t')\, r\, dr\, dt' \tag{10}$$

where $r(t)$ is the outer edge of the plasma at time $t$ and $t_0$ is the time at which the pressure at the center has decayed to the ambient pressure $p_0$. The first term of Eq. (10) is the one-dimensional contribution until the rarefaction reaches the center, and the second term is the contribution from the decaying pressure, which we treat in Sec. IV.

If pressure decay were instantaneous ($t_0 = \tau_H$), the second term would be absent and $I_r(t)$ would increase linearly with $\tau_p$ for $\tau_z \le \tau_R$ and be constant for $\tau_z > \tau_R$. Similarly, the coupling coefficient $I_r(t)/E$ would be constant for $\tau_z \le \tau_R$ and decrease $\propto \tau_p^{-1}$ for $\tau_z > \tau_R$. Hence the condition

$$\tau_z = \tau_R \tag{11}$$

represents the optimization condition for the pre-decay impulse, which simultaneously maximizes $I_r(t)$ and $I_r(t)/E$.

Using Eqs. (5-7), Eq. (11) becomes

$$\tau_p = [\gamma/(2\gamma+1)]\,\tau_R \tag{12}$$

or, with $\gamma = 1.18$, we get the minimum pulse length for optimization under these idealized conditions

$$\tau_{\min} = 0.351\ \tau_R \tag{13}$$

For the LASNEX calculation shown in Fig. 3, $\tau_{\min} = 3.67$ μsec.

Using the beam intensity and radius described in Sec. II, we have calculated with LASNEX the impulse delivered to the target (assumed infinite) for a variety of pulse lengths, integrating in time until $t = 500$ μsec. We have defined $I_s \equiv I_R(t)$, the impulse over the beam spot, and $I_T \equiv I_\infty(t)$, the total impulse over an infinite target. We see from Fig. 4 that $I_s/E$ and $I_T/E$ attain their maximum values for very short pulses, due to the impulse delivered by $p_{DW}$, but $I_s$ and $I_T$ are then quite small. Both $I_s$ and $I_T$ increase with increasing pulse length while $I_s/E$ and $I_T/E$ decrease but with extended plateau regions. To a fair approximation, both $I_s/E$ and $I_T/E$ are optimized when $\tau_p = \tau_{\min}$. Also since $I_s$ and $I_T$ level off at $\tau_p = \tau_R$, we can say that $I$ is optimized when $\tau_p = \tau_R$. This latter relation is in approximate agreement with Pirri's equation $\tau_p = \tau_{2D}$ where $\tau_{2D}$ is defined as the spot diameter divided by the detonation wave speed $D$.

In the remainder of this paper, we consider only "efficient" pulses, for which $\tau_p \ge \tau_{\min}$ and $\tau_H = \tau_R$. For these pulses, the LSD wave front has moved less than one beam diameter from the target at the time the pulse is switched off. At this time, the ratio of the length of the plasma to its radius is $D\tau_p/R$. For the case $\tau_p = \tau_{\min}$, $D\tau_p/R = (\gamma+1)/(2\gamma+1) = 0.65$ for $\gamma = 1.18$; for $\tau_p = \tau_R$, $D\tau_p/R = (\gamma+1)/\gamma = 1.85$.

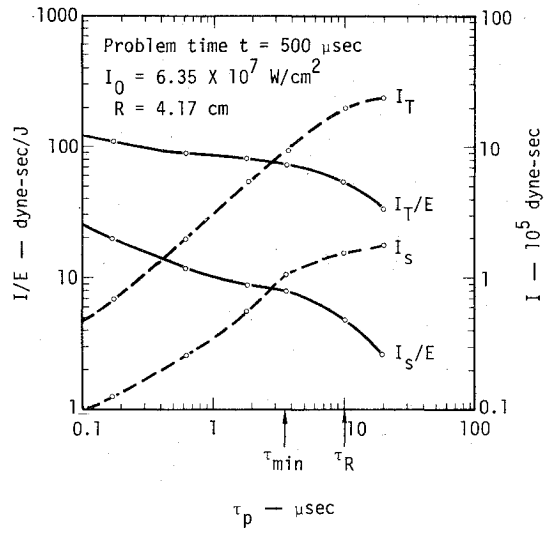


**Fig. 4 Coupling coefficient $I/E$ and impulse $I$ for spot and total loading vs pulse length for $t = 500$ μsec (LASNEX).**

## IV. Applicability of Blast Scaling Laws to Impulse Calculations

We have calculated the impulse delivered during the pressure decay, given by the integral in Eq. (10), and compared it to the blast-wave scaling models developed by Pirri[1] to determine the range of applicability of the latter. For spot loading, the impulse $I_s$ may be related to the impulse delivered by $p_{ID}$ up to the time $\tau_R$ when the pressure at the center begins to decrease. Calling this quantity $I_{s(\mathrm{ref})}$ we have

$$I_s = f I_{s(\mathrm{ref})} = f p_{ID} A_s \tau_R \tag{14}$$

where the ratio $f$, expected to be of order unity, represents the additional impulse delivered by the decaying pressure over the spot. Using a cylindrical blast-wave model and assuming that the pressure is uniform, we have

$$p(t) = \begin{cases} p_{ID} & t \le \tau_R \\ p_{ID}\tau_R/t & t > \tau_R \end{cases} \tag{15}$$

and

$$I_s = A_s p_{ID} \tau_R \left[1 + \int_{\tau_R}^{t_0} \frac{dt}{t}\right] \tag{16}$$

where $t_0$ is the time to reach ambient pressure. Hence we get

$$f_{\mathrm{cyl}} = 1 + \ln\frac{p_{ID}}{p_0} = 5.1 \tag{17}$$

for $p_{ID} = 110$ bars, $p_0 = 1$ bar.

Similarly, for a spherical blast-wave model $p(t) \propto t^{-6/5}$ and we have

$$f_{\mathrm{sph}} = 6 - 5\left(\frac{p_0}{p_{ID}}\right)^{1/6} = 3.7 \tag{18}$$

LASNEX calculations were made out to $t_0 = 500$ μsec. For comparison, $p_0$ in Eq. (17) becomes $2.2\,p_0$ and $p_0$ in Eq. (18) is approximately $p_0$. These corrections are reflected in Tables 2 and 3.

**Table 2 Ratio $f$ of impulse delivered to reference impulse at $t = 500$ μsec**

| Type of loading | Type of blast wave | Equation | | Value of $f$ as determined by LASNEX $\tau_p = \tau_{min}$ | $\tau_p = \tau_R$ | $\tau_p = 2\tau_R$ |
|---|---|---|---|---|---|---|
| Spot | Spherical | $6 - 5(p_0/p_{1D})^{1/6}$ | $= 3.7$ | 1.75 | 2.42 | 3.0 |
| | Cylindrical | $1 + \ln(p_{1D}/2.2p_0)$ | $= 4.9$ | | | |
| Total | Spherical | $5/3(p_{1D}/p_0) - 2/3$ | $= 16.8$ | 15.3 | 33 | 40 |
| | Cylindrical | $p_{1D}/2.2p_0$ | $= 55$ | | | |

**Table 3 Impulse scaling laws given $I = p_{1D} A_s \tau_R f$**

| Type of loading | Type of blast wave | $f$ | Time |
|---|---|---|---|
| Spot | Spherical | $0.5\left[6 - 5\left(\frac{p_0}{p_{1D}}\right)^{1/6}\right]$ | $\tau_{min} \le \tau_p < \tau_R$ |
| | Cylindrical | $0.5\left[1 + \ln\left(\frac{p_{1D}}{p_0}\right)\right]$ | $\tau_p \ge \tau_R$ |
| Total | Spherical | $\frac{5}{3}\frac{p_{1D}}{p_0} - \frac{2}{3}$ | $\tau_{min} \le \tau_p < \tau_R$ |
| | Cylindrical | $\frac{p_{1D}}{p_0}$ | $\tau_p > \tau_R$ |

where

$\tau_0 = 500$ μsec, $p_0 = \max\left[p_{1D}\left(\frac{\tau_R\,(\mu\text{sec})}{500}\right)^{6/5}, 1\right]$ for spherical loading

and $p_0 = \max\left[p_{1D}\frac{\tau_R\,(\mu\text{sec})}{500}, 1\right]$ for cylindrical loading

The values of $f$ calculated by LASNEX are significantly less than these theoretical values. For $\tau_p = \tau_{min}$ we find $f = 1.75$, and for $\tau_p = \tau_R$ we get $f = 2.42$. This suggests that a considerable part of the pressure decay over the spot could better be modeled as an isothermal expansion, with a rarefaction moving in from the outside of the spot toward the center. The pressure in the outer portion of the spot area, which represents most of the area, would thus decay sooner and more rapidly than the blast-wave rate.

Similar calculations can be carried out for total loading. For the spherical case we assume $r = R(t/\tau_R)^{2/5}$, $p = p_{1D}(\tau_R/t)^{6/5}$ for $t > \tau_R$; and for the cylindrical case $r = R(t/\tau_R)^{1/2}$, $p = p_{1D}(\tau_R/t)$. To determine the type of scaling relation that might be applicable, we have plotted $I_T$ vs $t$ for various pulse lengths in Fig. 5. The lines become straight after a time $t \approx 3\tau_p$, and the slopes of the graph of log $I_T$ vs log $t$ lie in the range $0.70 \pm 0.05$. For a spherical blast wave we would expect a value of 3/5 (Ref. 11) and for a cylindrical blast wave 1. A comparison of LASNEX with computed values for $f$ are given in Table 2 for various pulse lengths. For total loading, $f$ lies between the spherical and cylindrical blast-wave results, but closer to the former, as we would expect from the slope of the $I_T$-vs-$t$ curve. Thus the computational results indicate that spherical blast scaling overestimates the impulse for spot loading and is in agreement for total loading in the case $\tau_p = \tau_{min}$. Cylindrical blast scaling for total loading is more appropriate when $\tau_p \ge \tau_R$. We have summarized the impulse scaling laws in Table 3, based on calculations with $R = 4.17$ cm and $I_0 = 6.35 \times 10^7$ W/cm$^2$.

An important parameter for evaluating impulsive damage is the average impulse intensity $I/A$. Therefore, it is of interest to compare $I_s/A_s$, for spot loading, with $I_T/A_T$ for total loading ($A_s$ = spot area, $A_T$ = area of spreading hot plasma).

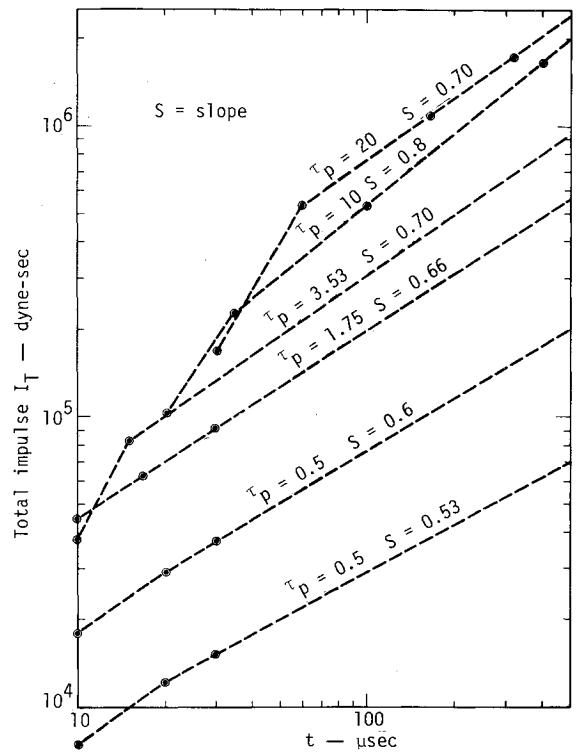


**Fig. 5 Total impulse vs time for various pulse lengths (LASNEX).**

For spot loading we have

$$I_s/A_s = f\, p_{1D} \tau_R \tag{19}$$

where $f = f(\tau_p)$.

For total loading we need to determine the area $A_T$ covered by the hot plasma at the time the pressure $p_{1D}$ has fallen to ambient pressure $p_0$. For a spherical blast-wave model[11]

$$r(t) = \xi_0 (2E/\rho_0)^{1/5} t^{2/5} \tag{20}$$

where $\xi_0 \approx 1$. We have inserted $2E$ in place of $E$ in Eq. (20) since we have a hemispherical blast wave due to the presence of the surface. As shown in Fig. 6, this formula agrees well with LASNEX calculations.

Taking $t = 500$ μsec as the time to reach ambient pressure we have for the radius $r_T$ at that time

$$r_T = 26.8[\tau_p\,(\mu\text{sec})]^{1/5}\text{cm} \tag{21}$$

Since $A_T = \pi r_T^2$, we can convert $I_T$ to $I_T/A_T$ for total loading as shown in Fig. 7. We see that $I_s/A_s$ exceeds $I_T/A_T$ by a factor of 6.

Figure 7 shows the impulse intensity as a function of radius for various pulse times. The average intensity over the spot can be represented by Eq. (19) with $f = 2.42$; i.e., $I_s/A_s = 2.42 \times 110 \times 10.5 = 2795$ dyne-sec/cm$^2$ for $\tau_p = \tau_R$.

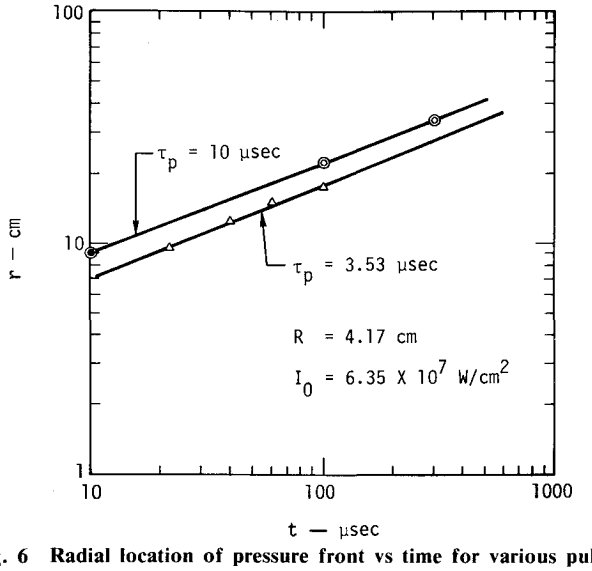


Fig. 6 Radial location of pressure front vs time for various pulse lengths (LASNEX).

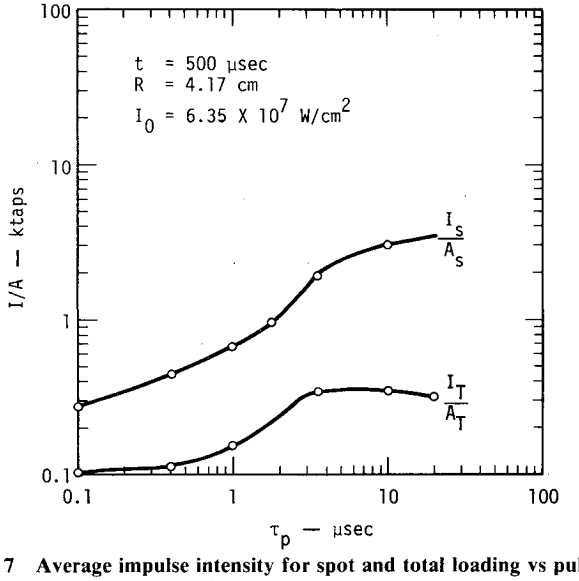


Fig. 7 Average impulse intensity for spot and total loading vs pulse length ($I_s$ taken from Fig. 5).

It is also of interest to note how well spherical and cylindrical blast-wave scaling match the calculated impulse intensity distribution. The impulse intensity is given by

$$I_I(r) = \begin{cases} p_{ID}\tau_R f & r \le R \\ \int_{t(r)}^{t_0} p(r,t)\, dt & r > R \end{cases} \tag{22}$$

For a cylindrical blast wave $p = p_{ID}(\tau_R/t)$, $t = \tau_R (r/R)^2$, and $t_0 = \tau_R (p_{ID}/p_0)$. Therefore

$$I_I(r)_{\text{cyl}} = p_{ID}\tau_R \ln\left(\frac{p_{ID}}{p_0}\frac{R^2}{r^2}\right) \quad \text{for} \quad r > R \tag{23}$$

For a spherical blast wave $p = p_{ID}(\tau_R/t)^{6/5}$, $t = \tau_R (r/R)^{5/2}$, and $t_0 = \tau_R (p_{ID}/p_0)^{5/6}$. Then

$$I_I(r)_{\text{sph}} = p_{ID}\tau_R\left[5\left(\frac{R}{r}\right)^{1/2}\left(\frac{p_0}{p_{ID}}\right)^{1/6}\right] \quad \text{for} \quad r > R \tag{24}$$

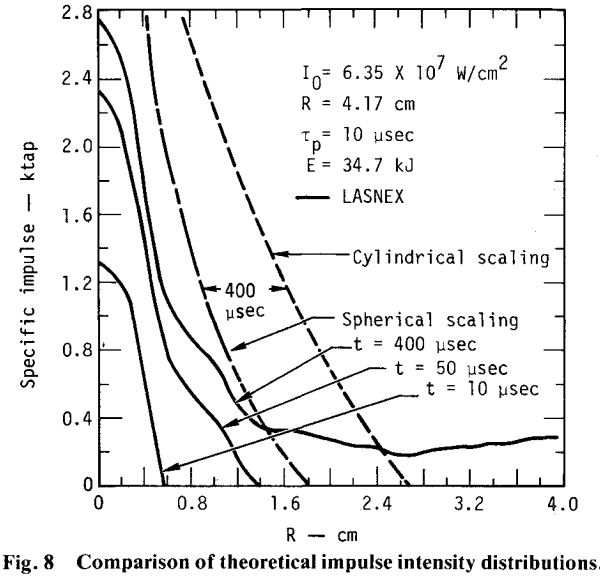


Fig. 8 Comparison of theoretical impulse intensity distributions.

A comparison of these results with LASNEX calculations for $t = 400$ μsec is shown in Fig. 8. Since $t_0 = 400$ μsec, $p_0$ in Eq. 23 becomes $2.88\,p_0$ and $p_0$ in Eq. 24 becomes $1.4\,p_0$. The results show that the scaling laws do poorly in describing the impulse-intensity distribution.

A further comparison with previous LASNEX results[3] is shown in Figs. 9 and 10 for $I_0 = 3\times10^9$ W/cm$^2$, $R = 2.5$ cm, $\tau_p = 5.73$ μsec, $t = 25$ μsec, $\tau_R = 1.77$ μsec, $p_{ID} = 1435$ bars and $p_{DW} = 4057$ bars, $(p_0)_{\text{cyl}} = 100$ bars, $(p_0)_{\text{sph}} = 60$ bars, $f_{\text{cyl}} = 3.66$, and $f_{\text{sph}} = 3.0$. In Fig. 9, the dominant effect is the detonation pressure near the surface for large-intensity pulses. Figure 10 shows that cylindrical blast scaling overestimates the impulse intensity over the spot but gives reasonable results for the spreading at early times.

## V. Optimized Beam and Target Parameters for Spot Loading

A pulsed laser beam with uniform intensity is characterized by three parameters, e.g., $I_0$, $\tau_p$, and $R$, which determine other beam quantities such as pulse energy $E = I_0\pi R^2\tau_p$ and spot impulse $I_s = fp_{ID}\pi R^2\tau_R$. Similarly a circular target may be described by two parameters: target radius $a$, and impulse to failure $I_f$.

For efficient impulse delivery, these five parameters are not independent, but are subject to three constraints:

1) Pulse optimization: $\tau_p = \tau_{\min}$ [Eq. (12)]. This condition is chosen to optimize $I_s/E$ (alternatively we could have chosen $\tau_p = \tau_R$ to optimize $I_s$).

2) Minimum impulse: $I_s = I_f$ delivering the minimum impulse required to produce target failure. For the particular case of thin ductile circular plates, we have shown[4,5] that $I_f = K\pi a^2 T$ where $T$ is the plate thickness and $K$ is a constant characteristic of the plate material. The fracture criteria for brittle plates are discussed by Colton.[12]

3) Matching beam radius to target radius: $R = a$. This may be derived as follows. Consider the effect on $I$, the impulse delivered to the target of area $\pi a^2$, of varying the beam radius $R$ keeping the pulse energy $E$ fixed. First assume $R \le a$. Then $E \propto I_0 R^2\tau_p \propto I_0^{1/3} R^3$ for optimized pulses, whereas $I \propto p_{ID}R^2\tau_p \propto I_0^{1/3} R_\infty^3 E^{1/2} R^{3/2}$. Hence, $I \propto (R/a)^{3/2}$ for $R \le a$. Now consider the case $R \ge a$. Then $I \propto p_{ID}a^2\tau_p \propto I_0^{1/3} R \propto E^{1/2}/R^{1/2}$. Hence, $I \propto (a/R)^{1/2}$ for $R \ge a$, and in both cases $I$ is maximized when $R = a$. For the case $R \le a$, the effect of plasma spreading weakens the dependence on $R$ somewhat.

When these conditions are imposed, the laser beam parameters required to rupture a given target are completely determined by any two of the five beam and target parameters. For example, choosing $I_0$ and $\tau_p$ as the in-

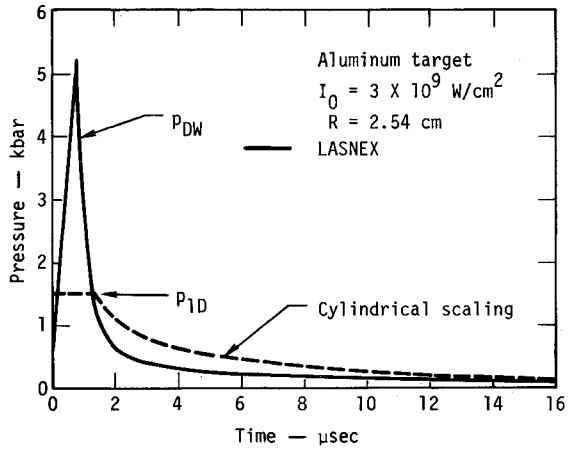


**Fig. 9 Comparison of theoretical surface pressure histories at beam center.**

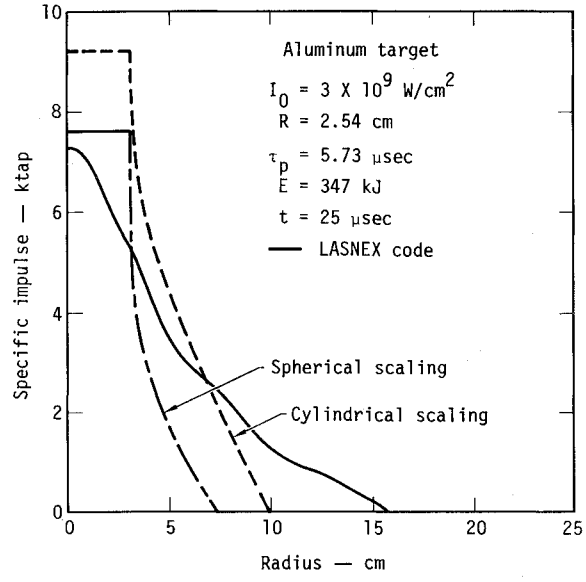


**Fig. 10 Comparison of theoretical impulse intensity distributions.**

dependent parameters we obtain

$$R=c_1 I_0^{1/3}\tau_p \quad I_s/A_s=c_2 I_0^{1/3}\tau_p \quad E/A_s=I_0\tau_p \tag{25}$$

where

$$A_s\equiv\pi R^2$$

$$c_1\equiv\left(\frac{2\gamma+1}{\gamma+1}\right)\left[\frac{2(\gamma^2-1)}{\rho_0}\right]^{1/3}$$

$$c_2=\frac{(2\gamma+1)}{\gamma(\gamma+1)}\left(\frac{\gamma+1}{2\gamma}\right)^{2\gamma/\gamma-1}[2(\gamma^2-1)]^{2/3}\rho_0^{1/3}f$$

$$f=0.5\left[6-5\left(\frac{p_0}{p_{1D}}\right)^{1/6}\right] \tag{26}$$

Using cgs units for the variables in Eqs. (25), and taking $\gamma=1.18$, we find that Eqs. (26) become

$$c_1=13.20(0.00125/\rho_0)^{1/3}$$

$$c_2=0.08461(\rho_0/0.00125)^{1/3}f$$

$f\approx 1.75$ based on the LASNEX calculation of Sec. IV(27)

For the case $\tau_p=\tau_R$, $c_1$ and $c_2$ must be multiplied by $\gamma/(2\gamma+1)$, and $f=0.5[1+\ln(p_{1D}/p_0)]$.

Some other useful pairs of beam parameters, and the resulting equations obtained from Eqs. (25-27), are given below:

1) $I_0$ and $E$:

$$\tau_p=(\pi c_1^2)^{-1/3}E^{1/3}I_0^{-5/9}$$

$$R=(c_1/\pi)^{1/3}E^{1/3}I_0^{-2/9}$$

$$I_s/A_s=c_2(\pi c_1^2)^{-1/3}E^{1/3}I_0^{1/9} \tag{28}$$

2) $I_0$ and $R$:

$$\tau_p=c_1^{-1}RI_0^{-1/3}$$

$$I_s/A_s=c_2c_1^{-1}RI_0^{1/3}$$

$$E=\pi c_1^{-1}R^2I_0^{1/3} \tag{29}$$

3) $I_0$ and $I_s/A_s$:

$$\tau_p=c_2^{-1}(I_s/A_s)I_0^{-1/3}$$

$$R=c_1c_2^{-1}(I_s/A_s)I_0^{-1/3}$$

$$E=\pi c_1^2c_2^{-3}(I_s/A_s)^3I_0^{-1/3} \tag{30}$$

From these results we obtain the optimized beam parameters given in Table 4 for a laser capable of delivering 10 ktap to a target, sufficient to rupture 3.1 mm of aluminum or 0.7 mm of stainless steel.

It will be noted that less energy is needed at higher intensities, even though laser coupling goes down with increasing intensity. This is because pressure increases more rapidly as a function of increasing intensity than coupling decreases. Thus pressure does not need to be maintained as long for a given value of $I_r$, and the spot radius $R$ and the

**Table 4 Optimized laser beam parameters yielding $I_s/A_s = 10^4$ taps**

| $I_0$ (W/cm$^2$) | $\tau_p$(μsec) | $E$(MJ) | $R$(cm) | $I_s$ ($10^6$ dyne-sec) | $I_s/E\left(\frac{\text{taps}}{\text{J/cm}^2}\right)$ | $E/A_s$(J/cm$^2$) |
|---|---|---|---|---|---|---|
| | | | $\rho_{air}=\rho_0$ | | | |
| $10^7$ | 73.0 | 4.4 | 44.7 | 62.8 | 14.3 | 697 |
| $10^8$ | 15.7 | 2.1 | 20.7 | 13.5 | 6.3 | 1582 |
| $10^9$ | 3.4 | 1.0 | 9.6 | 2.9 | 2.9 | 3453 |
| | | | $\rho_{air}=0.1\,\rho_p$ | | | |
| $10^7$ | 157 | 214 | 207 | 1346 | 6.3 | 1589 |
| $10^8$ | 33.9 | 99 | 96 | 289 | 2.9 | 3419 |
| $10^9$ | 7.3 | 46 | 45 | 63 | 1.4 | 7230 |

total energy can be correspondingly reduced. On the other hand, the higher energy pulses associated with the lower fluxes result in a greater total momentum delivery to the target, which may be an advantage.

The scaling of the laser parameters with ambient density $\rho_0$ is determined by Eq. (27), which shows that $c_1 \propto \rho_0^{1/3}$, $c_2 \propto \rho_0^{-1/3}$. Thus if $I_0$ and $I_s/A_s$ are taken as independent parameters as in Eq. (30), we see that $\tau_p \propto \rho_0^{-1/3}$, $R \propto \rho_0^{-1/3}$, $E \propto \rho_0^{-5/3}$. The pulse energy $E$ increases rapidly as $\rho_0$ is decreased, i.e., at higher altitudes. This is shown in Table 4 where we present the same beam parameters for $\rho_0 = 1.25 \times 10^{-4}$ g/cm$^3$, i.e., at air density equal to 0.1 of sea-level air density. Since $E \propto \rho_0^{-5/3}$, we see that the energy requirements at higher altitudes are greatly increased, whereas at the same time the coupling coefficient is reduced and the beam size increased. Thus damage by LSD waves will be less feasible at high altitudes.

## VI. Conclusions

Our numerical calculations have shown the following:

1) The pressure history on the target surface shows two characteristic relaxation times, which we explain in terms of simple radial and axial relaxation.

2) The impulse delivered and the coupling coefficient can be optimized as functions of pulse length based on the characteristic relaxation times; the resulting rules are a) $\tau_p = \tau_{\min}$ optimizes $I/E$ and b) $\tau_p = \tau_R$ optimizes $I$.

3) Blast-wave scaling for the pressure decay overestimates the impulse under the beam spot but gives reasonable results for total loading. The impulse-intensity distribution over the target is difficult to describe by scaling laws since blast scaling does not apply in the region over the spot or at low pressures. It is surprising that the total impulse calculation agrees reasonably well.

4) Spot loading, in which the beam radius is made equal to the target radius, delivers more impulse per unit area than does total loading in which plasma spreading is used to deliver impulse outside the beam spot.

Using optimized pulses with minimum impulse and matched radii, any two beam or target parameters, such as intensity and pulse length or pulse energy and radius, determine all the other parameters. For aluminum and stainless steel plates a few millimeters thick, we show that (at sea level) pulse lengths 8-40 $\mu$sec, beam radii 10-20 cm, and pulse energies 0.3-0.6 MJ for intensities $10^7$-$10^8$ W/cm$^2$ are required. At high altitude ($\sim$20 km) the requirements are more severe: pulse lengths 20-80 $\mu$sec, beam radii 50-110 cm, and pulse energies 12-30 MJ. These high energy requirements may seriously limit the high-altitude usefulness of high-power lasers operating through LSD waves.

## Acknowledgment

This research was performed under contract to the Advanced Research Projects Agency of the Depeartment of Defense, under the auspices of the U.S. Energy Research and Development Administration under contract No. W-7405-Eng-48.

## References

[1] Pirri, A.N., "Theory for Momentum Transfer to a Surface with a High-Power Laser," *Physics of Fluids,* Vol. 16, 1973, pp. 1435-1440.

[2] Nielsen, P.E., "Hydrodynamic Calculations of Surface Response in the Presence of Laser-Supported Detonation Waves," *Journal of Applied Physics,* Vol. 46, Oct. 1975, pp. 4501-4505.

[3] Edwards, A., Ferriter, N., Fleck, J.A. Jr., and Winslow, A.M, "A Theoretical Description of the Interaction of a Pulsed Laser and a Target in an Air Environment," Lawrence Livermore Laboratory, Livermore, Calif., UCRL-51489, Nov. 1973.

[4] Ferriter, N., Maiden, D.E., Winslow, A.M., and Fleck, J.A. Jr., "Analysis of Efficient Impulse Delivery and Plate Rupture by Laser-Supported Detonation Waves," Lawrence Livermore Laboratory, Livermore, Calif., UCRL-51836, June 1975.

[5] Maiden, D.E. and Winslow, A.M., "A Simple Analysis of Large Deflections and Rupture of Circular Plates Under Impulsive Loading," Lawrence Livermore Laboratory, Livermore, Calif., UCRL-78279, May 1976.

[6] Hall, R., "An Investigation of Laser-Supported Detonation Waves," The Boeing Company, Seattle, Washington, AFWL-TR-73-28, June 1973.

[7] Raizer, Y. P., "Heating of a Gas by a Powerful Light Pulse," *Soviet Physics JETP,* Vol. 21, 1975, pp. 1009-1017.

[8] Stanyukovich, K.P., *Unsteady Motion of Continuous Media,* Pergamon Press, New York, 1960, p. 335.

[9] Holmes, B.S., "Explosive Simulation of LSD-Induced Loads," Stanford Research Institute, Menlo Park, Calif., SRI-3-4263, Jan. 1973.

[10] Hettche, L.R., Tucker, T.R., Schriempf, J.T., Stegman, R.L., and Metz, S.A., "Mechanical Response and Thermal Coupling of Metallic Targets to High-Intensity 1.06$\mu$ Laser Radiation," ASME Pub. 75-WA/HT-40, Dec. 1976.

[11] Zel'dovich, Y. B. and Raizer, Y.P., *Physics of Shock Waves and High Temperature Hydrodynamic Phenomena,* Vol. 1, Academic Press, New York, 1966, pp. 93-100.

[12] Colton, J.D., "Multiple Fracture of Plates Under Localized Impulsive Loading," *Journal of Applied Mechanics,* March 1976, pp. 33-38.